Downlink Performance of Optical Power Domain NOMA for Beyond 5G Enabled V2X Networks

Gurinder Singh, Anand Srivastava, Vivek Ashok Bohara, and Zilong Liu

Abstract—In this work, we explore the potential benefits and practical challenges associated with implementation of optical power domain non-orthogonal multiple access (OPD-NOMA) scheme for visible light communications (VLC) based vehicle-to-everything (V2X) networks with a major aim of providing vehicles with reliable, ubiquitous, and massive connectivity. In the proposed framework, an installed light source (e.g., traffic lamp post or street light lamp post) broadcasts a safety related message to desired nodes through visible light. However, such VLC transmission is subject to interference originating from the vehicles in the adjacent lane. Using the stochastic geometry approach, we model the locations of vehicles on the road via Poisson point process. We investigate the applicability of downlink OPD NOMA enabled V2X network for typical infrastructure-to-vehicle (I2V) communication in presence of interference caused from concurrent vehicle-to-vehicle (V2V) transmissions with an aid of stochastic geometry. Through the obtained results, it has been shown that the downlink OPD NOMA based V2X network offers improved performance in terms of outage performance and average achievable rate as compared to the conventional RF based V2X communication.

Index Terms—Intelligent Transportation System, Visible Light Communications (VLC), Vehicle-to-Everything (V2X), Stochastic Geometry.

I. Introduction

ACCORDING to 2020 survey statistics on road traffic injuries, issued by World Health Organization (WHO), the number of annual road traffic deaths has reached 1.35 millions. To address this global issue, it is crucial to investigate and deploy a wide range of intelligent transportation system (ITS) mechanisms such as dissemination of cooperative awareness messages (CAMs) or basic safety messages (BSMs) to prevent and reduce road accidents. These messages, currently delivered with the aid of traditional radio frequency (RF) based V2X technology currently, may become unaffordable due to the increasingly congested and expensive RF spectrum. Compounding the problem further is the limited RF spectrum which may not be able to cater for the growing demands for future ITS. Moreover, conventional RF based vehicular networking tends to become incompetent in dense traffic scenarios as it suffers from higher interference, longer communication delays, and lower Packet Reception Probability (PRP) when hundreds of vehicles located in the same neighbourhood try to communicate simultaneously.

Gurinder Singh, Anand Srivastava, and Vivek Ashok Bohara are with the Department of Electronics and Communications Engineering, IIIT-Delhi, New Delhi, India (E-mail: {gurinders, anand, vivek.b}@iiitd.ac.in). Zilong Liu is with the School of Computer Science and Electronics Engineering, University of Essex, UK (E-mail: zilong.liu@essex.ac.uk).

Against this background, visible light communication (VLC) offers an economically viable solution to implement Vehicle-to-everything (V2X) communications. Vehicular-Visible Light Communication (V-VLC) provides optical communication among vehicles using low-cost Light-Emitting Diodes (LEDs) and photo diodes. The use of optical bands complementary to RF is a promising technique to alleviate the problems caused by spectrum crunch in RF-based wireless communication [1]. For instance, in 5G and beyond (presumingly 6G), it is anticipated that autonomous vehicles will be served at extraordinarily high data rates and with extremely low latency [2]. The ultra-high data rates (potentially up to 100 Gbps) achieved by LED based VLC and its inherent features such as lower power consumption, lower cost, less complex transceiver design, enhanced security, less delay, higher packet reception rate and anti-electromagnetic interference make VLC technology an ideal candidate for future ITS in beyond 5G V2X networks.

The next generation vehicular network will also require reliable massive connectivity and reduced resource collision, hence a suitable multiple access (MA) scheme should be adopted that can cater for these requirements. Recently, Non-Orthogonal Multiple Access (NOMA) scheme has emerged as favourable multiple access scheme for next generation cellular networks. Compared to other multiple access techniques, NOMA provides higher spectral efficiency, better connectivity, user fairness, reduced latency and enhanced data rates which also makes it a strong contender for future development of vehicular networks [3]. NOMA allows multiple users to share the same channel resource via power domain or code domain multiplexing. Authors in [4] introduced NOMA techniques in power and code domains for long term evolution (LTE)-based vehicular networks to support reduced resource collision and massive connectivity.

Apart from its applications in conventional RF based communications, the performance of Optical Power Domain-NOMA (OPD-NOMA) based VLC systems has been widely investigated in [5]–[9]. PD-NOMA [10] multiplexes the users in power domain by assigning them with different power levels and applies the iteration-based Successive Interference Cancellation (SIC) to detect multiple signal streams at the receiver [11], [12]. It is shown in [12] that PD-NOMA is capable of improving the resource utilization efficiency in both uplink and downlink channels. To efficiently meet 6G-V2X requirements, the integration of VLC and NOMA is emerging as a disruptive technique for advanced use cases in connected autonomous vehicles [2].

A. Related Works

VLC may be considered as potential solution for high-speed and short-range wireless communications [13]. Together with recent development in light emitting diodes (LED) as the illumination source, VLC networks offers as an economically viable solution for simultaneous communication and illumination [14]–[16]. 5G networks and beyond need to guarantee services for a large number of high data-rate users that share the same resources. Recent research efforts reveal that V-VLC is capable of achieving a speed of more than multiple Gigabits per second [17], thus enabling the high data rate requirements in next generation wireless networks. In [6], [7] various power allocation schemes have been investigated for OPD-NOMA in order to maximize the sum average achievable rate. The experimental demonstrations of OPD-NOMA were reported in [7], [18], whereas applications of PD-NOMA in VLC were investigated [9], [19]. Most of existing state-of-the-art work on NOMA is primarily based on the assumption that the receiver is capable of performing perfect SIC, which means all the users can be perfectly decoded regardless the strengths of their individual channel fading gains. However, in practical system, there is error propagation in SIC receiver, also known as imperfect SIC, where weak users may suffer from certain interference residual due to incorrect decoding of the strongest users [20]–[22]. The effects of SIC imperfections have been studied in [21] for uplink multi carrier (MC)-NOMA based on virtualized wireless network (VWN). In [22], the joint resource allocation in NOMA system with perfect and imperfect SIC was investigated. The results showed that imperfect SIC leads to significant degradation of the performance of NOMA systems. As evident, most of the aforementioned works on NOMA-VLC considers an indoor environment. To the best of our knowledge, there is no literature available which provides comprehensive qualitative and quantitative analysis involved with employing OPD NOMA in vehicular communication scenarios.

In order to maintain the analytical tractability of the communication quality in ITS, we take the stochastic geometry approach, which is a powerful tool for modeling spatial random events in wireless communications [23]–[26]. For the purpose of analytical modeling, stochastic geometry [27] has been widely used in the last decade or so to understand the mathematical tractability and modeling accuracy of vehicular ad hoc networks (VANETs). For instance, in [28], the performance of IEEE 802.11p standard was investigated with the aid of a novel mathematical model based on queuing theory and stochastic geometry.

On one hand, NOMA has been considered for VLC networks in prior literature primarily focusing on indoor VLC channels [29] and [30]. On the other hand, RF based NOMA V2X networks have been studied in [31] and [32], aiming to address its feasibility and open challenges. However, none of these aforementioned studies presents an integration of NOMA into V-VLC network whose performance is severely affected by interference. In the proposed framework, we investigate the applicability of downlink OPD NOMA enabled V2X network for typical I2V communication in presence of interference

caused from other source transmissions. To the best of our knowledge, our presented work pioneers the modelling of stochastic behaviour of interference for such NOMA enabled V-VLC networks with the aid of stochastic geometry which has not been explored in the existing V2X-related literature. Further, we present an extensive comparison on performance of such OPD NOMA enabled V2X network with conventional V-RF communication (regulated by IEEE 802.11p standard).

B. Contributions

This research work aims to understand the potential benefits and practical challenges associated with employing downlink OPD NOMA based V2X network. The major contributions and findings of our work are summarized below:

- We explore the potential benefits of downlink NOMA using VLC in vehicular scenario for broadcasting road safety related information. We carry out performance analysis of the proposed downlink OPD NOMA based V2X network against the OMA counterpart with aid of stochastic geometry tools. This is carried out by considering the impact of interference from other vehicular transmission by V2V at the receiving nodes.
- We develop a novel tractable framework in terms of outage probability and achievable rate as performance metrics when a light source (e.g., traffic lamp post) transmits a message to two destination vehicles through visible light by assuming both perfect SIC and imperfect SIC decoding at the receiver.
- In order to verify the efficacy of the proposed OPD-NOMA technique, we compare the performance of downlink OPD NOMA based V2X network with conventional RF NOMA based V2X network. Depending upon the locations of NOMA users from source, we illustrate the trade-offs between these two different technologies.

C. Paper Organization and Notations

1) Paper Organization: The organization of the paper is as follows: Section II describes the network model and assumption used for analysis. Section III presents detailed analytical framework to characterize the downlink performance of OPD NOMA based V2X network in terms of outage probability and average achievable rate using various analytical tools of stochastic geometry. In Section IV, the simulation results and discussion are presented with useful insights and comments. Finally, concluding remarks are given in Section V.

2) Notations: $\mathbb{P}[\cdot]$ denotes the probability of an event, $||\cdot||$ denotes euclidean norm, $\mathbb{E}_Y[\cdot]$ is the expectation of its argument over random variable (RV) Y and $\mathscr{L}$ denotes Laplace transform of a function. $\mathbb{R}^1$ denotes one dimensional space. $\xi_c(\cdot), \varphi_X$ $\mathcal{F}_X(\cdot)$, $f_X(\cdot)$ and denote the complementary error function, characteristic function of an RV X, cumulative distribution function and its corresponding probability density function respectively.

II. System Model and Preliminaries

A. System Model

We consider an uni-directional traffic stream wherein either NOMA enabled VLC or RF downlink exists between road side unit (RSU) (mounted on LED traffic lamp) and vehicles as depicted in Fig.1. We assume that a light source (e.g., traffic lamp post) sends a message to destination nodes through visible light. However, such VLC transmission is subject to interference originating from neighbouring vehicles that are located on the roads. At transmitter side, as shown in Fig. 2, light source transmits the composite signal, which is a superposition of desired optical signals of user pairs with different power allocation. We consider the existence of a central information center (CIC) that collects and keeps track of some key system information (such as location and speed of each vehicle, road condition, BSMs dissemination) about the on-road vehicles. The communication between LED Traffic light and CIC is established via back-haul connectivity and to vehicles through free-space optical wireless transmission. For ease of understanding, Fig. 3 provides the schematic layout of proposed system model.

Fig. 1: Typical I2V and V2V-VLC scenario.

Fig. 2: OPD NOMA based V2X system model.

We consider a set of interfering vehicles which are distributed according to a one-dimensional homogeneous Poisson point process (1D-HPPP), represented as $\Psi_{PPP} \backsim$ 1D-

Fig. 3: Abstraction used for modelling. The desired vehicles are marked in triangle, while interferers are marked in cross marks. Here, L and h denotes the inter lane distance and height of traffic lamp respectively.

HPPP(λ, r), where r and λ denote the positions of the interferer vehicles and their intensity, respectively. Further, we assume that interfering vehicles follow Aloha MAC protocol with parameter ϱ, i.e., every node can access the medium with an access probability, ϱ [33]. We considered low speed vehicles (LSV) mobility model where we assume that interferer vehicles do not move or move slowly, that is, their positions remain the same during the two time slots of the transmission [34]. The proposed work is also in line with previous work proposed in [35] and [28]. The Doppler shift and time-varying effect of V2V and V2I channel on the performance of OPD-NOMA enabled V2X networks has been left as a subject of future investigation.

B. Channel Model for V-VLC and V-RF

We consider an outdoor VLC downlink transmission scenario which involves a single transmitting LED traffic lamp and k nodes each of which is equipped with a photodetector for signal reception. It is assumed that k nodes are within the coverage area of transmitting LED. For such I2V-VLC system, the direct current (DC) VLC channel gain can be represented as [36]

$$h_k = \frac{(m+1)A_R}{2\pi D_k^\gamma} \cos^m(\phi_k) \cos(\Psi_k) T_s(\Psi_k) g(\Psi_k), \quad (1)$$

where A_R, Ψ_k and ϕ_k denote the area of photodetector (PD), the angle of arrival (AoA) and the angle of irradiance respectively. $T_s(\Psi_k)$ denotes the gain of the optical filter at the receiver; $g(\Psi_k)$ denotes the gain of optical concentrator at the receiver front-end which is given as

$$g(\Psi_k) = \begin{cases} \frac{n^2}{\sin^2 \Psi_{FOV}}; & \text{if } 0 \leq \phi_k \leq \Psi_{FOV}, \\ 0; & \text{if } \phi_k > \Psi_{FOV}, \end{cases} \quad (2)$$

where n denotes the refractive index of the optical concentrator and D_k denotes the Euclidean distance between the kth vehicle and RSU. Here, m is the order of the Lambertian model and is given by $m = -\frac{\ln(2)}{\ln\left(\cos\left(\phi_{\frac{1}{2}}\right)\right)}$. For a RF link, we assume that the amplitude of received signal follows Rayleigh distribution.

Hence, the channel fading gain (h_k) is an exponential random variable (r.v.).

C. Practical Challenges

In order to achieve the same quality of service (QoS) for each received signal, we derive the general formula for the transmit power level required for each vehicular node. With no loss of generality, let us consider that a NOMA group consists of k vehicles, which are categorized based on their channel gain conditions in ascending order as $h_1 \leq h_2... \leq h_k$. Based on such ordering, NOMA technique can permit V_i to decode the interfering NOMA signals originating from V_k, $k \leq i$ and then eliminate the interfering NOMA signals from the received signal, in a successive manner. According to the NOMA principle and the order of channel gains, power P_i is allocated in descending order, i.e., $P_1 \geq ... \geq P_k$, which is reverse to the order of h_i.

The received optical signal at V_i can be represented as

$$y_i = \mathcal{R}h_i s + n, \qquad (3)$$

where s denotes composite optical transmitted from LED, $\mathcal{R}$ denotes the responsivity of PD, n denotes the additive white Gaussian noise with zero mean and variance, σ^2. We assume that there is a perfect interference cancellation through SIC at the each receiving node. Hence, the SIC enabled receiver first decodes the strongest signal and then subtracts it from the composite received signal. This process continues until all the signals are properly detected. Due to non-uniform power allocation at all the transmitting vehicles, OPD-NOMA with SIC exploits the signal-to-interference plus noise ratio (SINR) difference among vehicles. It is assumed that the required electrical SINR, γ at each receiving node is same (say, constant, c). Mathematically,

$$\gamma = \frac{(\mathcal{R}P_{r_k})^2}{\sigma_k^2} = c \qquad \forall k, \qquad (4)$$

where P_{r_k} denotes optical power received from the k-th vehicle. The transmitter power, P_1 is set such that symbol s_1 can be received accurately, that is

$$P_{r1} = \frac{\sigma_1}{\mathcal{R}}\sqrt{\gamma},$$
$$P_1 = \frac{\sigma_1}{\mathcal{R}h_1}\sqrt{\gamma}. \qquad (5)$$

The same can be extended for the vehicle V_2 transmitter power P_2 which is computed as:

$$\gamma = \frac{(\mathcal{R}P_{r_2})^2}{(\mathcal{R}P_{r_1})^2 + \sigma_2^2},$$
$$P_{r2} = \frac{\sigma_2}{\mathcal{R}}\sqrt{\gamma(\gamma+1)}, \qquad (6)$$
$$P_2 = \frac{\sigma_2}{\mathcal{R}h_2}\sqrt{\gamma(\gamma+1)}.$$

This approach is iteratively applied to determine vehicle V_3 transmit power, P_3, which depends on the past values of P_1 and P_2 and can be given in simplified form as

$$P_3 = \frac{\sigma_3}{\mathcal{R}h_3}\sqrt{\gamma(\gamma^2 + 2\gamma + 1)}. \qquad (7)$$

In general, the same concept can be extended to N transmitting vehicles. Further, the transmit power for the i-th vehicle can be given as a function of the noise variance σ_i, channel gain coefficient h_i, and the required SINR[1] as

$$P_i = \frac{\sigma_i}{\mathcal{R}h_i}\sqrt{\gamma}(\gamma+1)^{\frac{i-1}{2}}, i = 1, 2, 3, .., N. \qquad (8)$$

For transmitting information in power domain, recognising that vehicle V_i has worse channel conditions, PD-NOMA allocates a greater amount of power P_i to that vehicle depending on channel conditions. Thus, there exists non-uniform transmit power allocation among vehicles which is critical for designing a practical V-VLC system. Several open issues such as power imbalance and maintaining fairness among vehicles need to be addressed carefully before practical deployment of OPD-NOMA to vehicular communication systems. Further, in the OPD-NOMA downlink, the unavailability of channel state knowledge impacts the overall system performance, since the channel state information (CSI) for each vehicular node must be known by all users and the light source allocates power to each vehicular node based on its CSI which brings further challenges for NOMA implementation in vehicular scenario.

III. PERFORMANCE ANALYSIS

For the sake of analysis, we specifically consider interference limited scenario wherein two vehicular nodes, V_1 and V_2 are selected to perform NOMA jointly since asking all the vehicles in network to participate is not preferable in practice. However, the proposed analysis can be easily extended to a generic NOMA scheme with M vehicles, $M \geq 2$. We also consider that the receiving vehicular nodes are sorted according to their preset QoS priorities [37], [38]. In other words, V_1 has to be served immediately with a lower data rate whereas V_2 needs a higher data rate but can be served later. Even in real life, not all users require the same amount of data rate. Let the signals intended to V_1 and V_2 are denoted as x_1 and x_2, respectively, where $\mathbb{E}[|x_i|^2] = 1$. As per NOMA principle [12], the transmitted optical signal from LED is coded as the composite signal from V_1 and V_2,

$$x = \sqrt{P_1}x_1 + \sqrt{P_2}x_2. \qquad (9)$$

Thus the received signal at V_i can be represented in an interference limited system as

$$y_i = \mathcal{R}h_i x + \sqrt{\mathcal{I}_i}. \qquad (10)$$

In following subsection, we derive analytical expression for NOMA outage probability and average achievable rate for two-vehicular case.

A. NOMA Outage Expression for V-VLC

An outage is said to occur when the instantaneous SINR falls below a certain SINR threshold. For V-VLC, noise variance is negligible as compared to aggregate interference [39].

---

[1]Note that the transmit power allocation adopted among vehicles is critical for a practical V-VLC system design. For sake of analysis, we assume that each vehicle is allocated power more than certain minimum threshold power which can suffice illumination as well as communication constraint.

For such interference limited scenario, we first calculate the signal-to-interference ratio (SIR) at each receiving vehicular node, then define outage probability associated to them. As V_1 is assumed to be received with higher power, therefore it will be firstly decoded according to SIC decoding. Subsequently, interference would be V_2, and SIR at V_1, denoted as SIR_{V_1}, can be expressed as

$$SIR_{V_1} = \frac{k\xi_1 P_{VLC} r_1^{2(m+1)} ||h^2 + r_1^2||^{-(m+\gamma+1)}}{k\xi_2 P_{VLC} r_1^{2(m+1)} ||h^2 + r_1^2||^{-(m+3)} + \mathcal{I}_{\mathcal{VLC}}}. \tag{11}$$

In [11], ξ_1, and P_{VLC} denote the power allocation coefficient associated with vehicle, V_1 and the transmission power for VLC respectively. $\mathcal{I}_{\mathcal{VLC}}$ denotes the aggregate interference experienced at the receiving node from vehicles in adjacent lane (VLC-V2V). Referring to Fig. 3, we can deduce $cos(\phi) = cos(\psi) = \frac{r'}{\sqrt{(L^2+r'^2)}}$ for given system model based on simple geometrical argument. The interference $\mathcal{I}_{\mathcal{VLC}}$ can be given as

$$\mathcal{I}_{\mathcal{VLC}} = \sum_{i=1}^{N} k \frac{r_i'^{2(m+1)}}{(L^2 + r_i'^2)^{(m+3)}} P_{VLC}; \tag{12}$$

Here $k = \left(\frac{\mathcal{R}(m+1)A_R}{2\pi} T_s(\psi)G(\psi)\right)^2$. In contrary, as V_2 comes second in decoding order, it has to first retrieve V_1 message, denoted as SIR_{V_2-1}, is expressed as,

$$SIR_{V_2-1} = \frac{k\xi_1 P_{VLC} r_2^{2(m+1)} ||h^2 + r_2^2||^{-(m+3)}}{k\xi_2 P_{VLC} r_2^{2(m+1)} ||h^2 + r_2^2||^{-(m+3)} + \mathcal{I}'_{\mathcal{VLC}}}. \tag{13}$$

The SIR at V_2 to decode its own message, denoted as SIR_{V_2}, is expressed as

$$SIR_{V_2} = \frac{k\xi_2 P_{VLC} r_2^{2(m+1)} ||h^2 + r_2^2||^{-(m+3)}}{\mu k\xi_1 P_{VLC} r_2^{2(m+1)} ||h^2 + r_2^2||^{-(m+3)} + \mathcal{I}'_{\mathcal{VLC}}}. \tag{14}$$

where $\mu \in (0,1)$ denotes residual factor accounting for interference fraction that remains due to imperfect SIC at the receiver. For the case of perfect SIC, $\mu = 0$. Let us denote outage event related to V_1 as O_{V_1}, which is expressed as

$$O_{V_1} = \{SIR_{V_1} < \beta_1\}, \tag{15}$$

where, $\beta_1 = \frac{2\pi}{e}(2^{2R_1} - 1)$ and R_1 is target data rate of V_1. At any NOMA receiver, the overall decoding mechanism is considered to be in outage if instantaneous user rates associated with either Eq.(11) or Eq.(14) do not suffice the respective target rates. Let O_{V_2-1} denote the outage event when V_2 cannot decode V_1 message, expressed as

$$O_{V_2-1} = \{SIR_{V_2-1} < \beta_1\}, \tag{16}$$

Now, let O_{V_2} denote the outage event when V_2 cannot retrieve its own message, expressed as

$$O_{V_2} = \{SIR_{V_2} < \beta_2\}, \tag{17}$$

where $\beta_2 = \frac{2\pi}{e}(2^{2R_2} - 1)$ and R_2 is target data rate of V_2. Having this background, we are now in position to calculate the outage probability related to V_1 and V_2. We make use of

moment generating functional (MGF) approach to solve for the outage probability.

V_1 **outage probability:**
$$\mathcal{P}_{O_{V_1}} =$$

$$\mathbb{P}\left(\frac{\mathcal{I}_{\mathcal{VLC}}}{k(\xi_1 - \beta_1\xi_2)P_{VLC} r_1^{2(m+1)} ||h^2 + r_1^2||^{-(m+3)}} > \frac{1}{\beta_1}\right). \tag{18}$$

Let us define random variable Z as

$$Z = \frac{\mathcal{I}_{\mathcal{VLC}}}{k(\xi_1 - \beta_1\xi_2)P_{VLC} r_1^{2(m+1)} ||h^2 + r_1^2||^{-(m+3)}} \tag{19}$$

Hence, (19) can be rewritten as

$$P_{out} = \mathbb{P}(Z > \beta^{-1}) = 1 - F_Z(\beta^{-1}). \tag{20}$$

In general, a closed-form solution for $F_Z(\beta^{-1})$ is quite difficult to obtain. Hence, we utilize numerical inversion of Laplace transform to find CDF, $F_Z(\beta^{-1})$. The CDF of a random variable Z is related to the Laplace transform of $F_Z(z)$ as [40]

$$F_Z(z) = \frac{1}{2\pi j} \int_{c-j\infty}^{c+j\infty} \mathcal{L}_{F_Z(z)} \exp(sw)ds. \tag{21}$$

where j is imaginary number ($\sqrt{-1}$). The above integral can be discretized to get a series using the trapezoid rule and then the infinite series can be truncated to get a finite sum using the Euler summation [40]. Also, $\mathcal{L}_{F_Z(z)}(s) = \frac{\mathcal{L}_Z(s)}{s}$. Eq.(20) can be approximated as

$$P_{out} \approx 1 - \frac{2^{-B} \exp(\frac{A}{2})}{\beta^{-1}} \sum_{b=0}^{B} \binom{B}{b} \sum_{c=0}^{C+b} \frac{(-1)^c}{D_c} Re\left\{\frac{\mathcal{L}_Z(s)}{s}\right\}. \tag{22}$$

where $D_c = 2$ (if $c = 0$) and $D_c = 1$ (if $c = 1, 2, 3,..$) and s=$\frac{(A+j2\pi c)}{2\beta^{-1}}$. The estimation error is controlled by three parameters A, B and C. Using the well established result given in [41], [40], in order to achieve an estimation accuracy of $10^{-\eta}$ (i.e., having the $(\eta - 1)$th decimal correct), A, B and C have to be at least equal ηln10, 1.243η-1, and 1.467η, respectively. Setting A=8ln10, B=11, C=14 achieves stable numerical inversion with an estimation error of 10^{-8}.

The Laplace transform of the probability distribution of a random variable can be computed as
$$\mathcal{L}_Z(s)=$$

$$\mathbb{E}_\mathcal{I}\left\{\exp\left(-\frac{s\mathcal{I}_{\mathcal{VLC}}}{k(\xi_1 - \beta_1\xi_2)P_{VLC} r_1^{2(m+1)} ||h^2 + r_1^2||^{-(m+3)}}\right)\right\} \tag{23}$$

$$= \mathbb{E}_r\left\{\prod_{i=1}^{N} \exp\left(-\frac{s}{k(\xi_1 - \beta_1\xi_2)P_{VLC} r_1^{2(m+1)} ||h^2 + r_1^2||^{-(m+3)}} \times \frac{kr_i'^{2(m+1)}}{(L^2 + r_i'^2)^{(m+3)}}\right)\right\}, \tag{24}$$

The expectation in Eq.(24) can be solved using probability generating functional Laplace (PGFL) defined for a homogeneous Poisson point process [24, Th 4.9].

$$\mathbb{E}_r \left\{ \prod_{i=1}^{N} \exp\left(-\frac{s}{k(\xi_1 - \beta_1\xi_2)P_{VLC}r_1^{2(m+1)}||h^2+r_1^2||^{-(m+3)}} \right. \right.$$
$$\left. \left. \times \frac{kr_i'^{2(m+1)}}{(L^2+r_i'^2)^{(m+3)}} \right) \right\}$$

$$= \exp\left[-\varrho\lambda \int_{r_1}^{\infty} \left(1 - \exp\left(-\frac{s}{k(\xi_1-\beta_1\xi_2)} \right. \right. \right.$$
$$\left. \left. \left. \times \frac{kr^{2(m+1)}}{P_{VLC}r_1^{2(m+1)}||h^2+r_1^2||^{-(m+3)}(L^2+r^2)^{(m+3)}} \right) \right) dr \right]. \tag{25}$$

V_2 outage probability
In order to calculate $\mathcal{P}_{O_{V_2}}$, we express $\mathcal{P}_{O_{V_2}}$ as a function of success probability, $\mathcal{P}_{O_{V_{2-1} \cap O_{V_2}}}^C$ that is

$$\mathcal{P}_{O_{V_2}} = 1 - \mathcal{P}_{O_{V_2}}^C = 1 - \mathcal{P}_{O_{V_{2-1} \cap O_{V_2}}}^C, \tag{26}$$

$$\mathcal{P}_{O_{V_{2-1} \cap O_{V_2}}}^C =$$
$$\mathbb{P}\left(\frac{\mathcal{I}'_{\mathcal{VLC}}}{k(\xi_1-\beta_1\xi_2)P_{VLC}r_2^{2(m+1)}||h^2+r_2^2||^{-(m+3)}} < \frac{1}{\beta_1}, \right.$$
$$\left. \frac{\mathcal{I}'_{\mathcal{VLC}}}{k(\xi_2-\beta_2\mu\xi_1)P_{VLC}r_2^{2(m+1)}||h^2+r_2^2||^{-(m+3)}} < \frac{1}{\beta_2} \right),$$
$$= \mathbb{P}\left(\frac{\mathcal{I}'_{\mathcal{VLC}}}{kP_{VLC}r_2^{2(m+1)}||h^2+r_2^2||^{-(m+3)}} < \frac{(\xi_1-\beta_1\xi_2)}{\beta_1}, \right.$$
$$\left. \frac{\mathcal{I}'_{\mathcal{VLC}}}{kP_{VLC}r_2^{2(m+1)}||h^2+r_2^2||^{-(m+3)}} < \frac{(\xi_2-\beta_2\mu\xi_1)}{\beta_2} \right),$$
$$= \mathbb{P}\left(\frac{\mathcal{I}'_{\mathcal{VLC}}}{kP_{VLC}r_2^{2(m+1)}||h^2+r_2^2||^{-(m+3)}} < \min(J_1, J_2) \right). \tag{27}$$

where $J_1 = \frac{(\xi_1-\beta_1\xi_2)}{\beta_1}$ and $J_2 = \frac{(\xi_2-\beta_2\mu\xi_1)}{\beta_2}$. Following same steps as (20)-(25), (26) can be solved using similar approach.
OPD-NOMA Extension to M-nodes
Now, we extend OPD NOMA results to M-destination nodes. The expression for SIR at node V_i to retrieve V_t message can be expressed as
$$SIR_{V_i \to t} =$$

$$\frac{k\xi_t P_{VLC}r_i^{2(m+1)}||h^2+r_i^2||^{-(m+3)}}{kP_{VLC}r_i^{2(m+1)}||h^2+r_i^2||^{-(m+3)}\left[\mu\sum_{k=1}^{t-1}\xi_k + \sum_{n=t+1}^{M}\xi_n \right] + \mathcal{I}_{VLC}^i} \tag{28}$$

Observe that, when $k > t-1$, then $\sum_{k=1}^{t-1}\xi_k = 0$ and when $n > M$, then $\sum_{n=t+1}^{M}\xi_n = 0$. In order to calculate outage probability

$\mathcal{P}_{O_{V_i}}$ at node V_i, we express a successful transmission at node V_i as

$$O_{V_i}^C = \bigcap_{n=M-i+1}^{M} \{ SIR_{V_i \to i-(M-n)} > R_{i-(M-n)}, \} \tag{29}$$

Finally, the outage probability can be expressed as
$\mathcal{P}_{O_{V_i}}$
$$= \begin{cases} 1; & \text{if } \bigcup_{t=1}^{M} \frac{\xi_t}{\mu\sum_{k=1}^{t-1}\xi_k + \sum_{n=t+1}^{M}\xi_n} < \beta_t, \\ 1 - \mathbb{P}\left(\frac{\mathcal{I}_{VLC}^i}{kP_{VLC}r_i^{2(m+1)}||h^2+r_i^2||^{-(m+3)}} < J_{(i)min} \right); & \text{otherwise,} \end{cases} \tag{30}$$

where $J_{(i)min}$ is given by
$J_{(i)min} =$

$$\min\left(\frac{\xi_{i-(M-1)} - \beta_{i-(M-1)}\left[\mu\sum_{k=1}^{i-(M-1)-1}\xi_k + \sum_{n=i-(M-1)+1}^{M}\xi_n \right]}{\beta_{i-(M-1)}}, \right.$$
$$\frac{\xi_{i-(M-2)} - \beta_{i-(M-2)}\left[\mu\sum_{k=1}^{i-(M-2)-1}\xi_k + \sum_{n=i-(M-2)+1}^{M}\xi_n \right]}{\beta_{i-(M-2)}}, ...,$$
$$\left. \frac{\xi_{i-(M-\ell)} - \beta_{i-(M-\ell)}\left[\mu\sum_{k=1}^{i-(M-\ell)-1}\xi_k + \sum_{n=i-(M-\ell)+1}^{M}\xi_n \right]}{\beta_{i-(M-l)}} \right). \tag{31}$$

where $\ell \in (1, 2,.., M)$. We set the condition that $\ell > M-i$. Intuitively, as the number of destination nodes, M increases, NOMA performance become better over OMA.

B. NOMA Outage Expression for V-RF
For V-RF, assuming free space path loss propagation model, the interference at the receiver can be given as aggregate of all the RF power received from N interferers as:

$$\mathcal{I}_{RF} = \sum_{i=1}^{N} P_{RF}G_tG_r\ell h_k||L^2+r_i'^2||^{-\frac{\alpha}{2}}, \tag{32}$$

Here, $\ell = \frac{c^2}{(4\pi)^2 f_0^2}$; c is speed of light and f_o is carrier frequency. In above expression, P_{RF}, α, G_t and G_r are the the RF transmission power, the path loss exponent, the antenna gains for transmitter and receiver respectively [42].
V_1 outage probability
The outage probability ($\mathcal{P}_{O_{V_1}}^{RF}$) related to V_1 in case of RF based vehicular communication can be given as.

$$\mathcal{P}_{O_{V_1}}^{RF} = 1 - \mathbb{P}\left(\frac{\xi_1 P_{RF}G_tG_r\ell h_1||h^2+r_1^2||^{-\frac{\alpha}{2}}}{\xi_2 P_{RF}G_tG_r\ell h_1||h^2+r_1^2||^{-\frac{\alpha}{2}} + \mathcal{I}_{RF}} > \zeta_1 \right),$$
$$= 1 - \mathbb{P}\left(h_1 > \frac{\zeta_1\mathcal{I}_{RF}}{(\xi_1-\zeta_1\xi_2)P_{RF}G_tG_r\ell||h^2+r_1^2||^{-\frac{\alpha}{2}}} \right),$$
$$= 1 - \left[\mathscr{L}_{I_{RF}}\left(\frac{\zeta_1}{(\xi_1-\zeta_1\xi_2)P_{RF}G_tG_r\ell||h^2+r_1^2||^{-\frac{\alpha}{2}}} \right) \right], \tag{33}$$

where $\zeta_1 = 2^{R_1} - 1$ and $\mathscr{L}(.)$ denotes for Laplace transform which is given as[2]

$$\mathscr{L}_{I_{RF}}\left(\frac{\zeta_1}{(\xi_1 - \zeta_1\xi_2)P_{RF}G_tG_r\ell||h^2 + r_1^2||^{-\frac{\alpha}{2}}}\right) =$$
$$\exp\left(-\varrho\lambda\left(\frac{\zeta_1}{(\xi_1 - \zeta_1\xi_2)}\right)^{\frac{1}{\alpha}} ||h^2 + r_1^2||^{\frac{1}{2}}\frac{\pi}{\alpha}\csc(\frac{\pi}{\alpha})\right). \quad (34)$$

Proof: Please refer to the **Appendix A**.

V_2 outage probability

As before, we express $\mathcal{P}_{O_{V_2}}^{RF}$ as a function of success probability, $\mathcal{P}_{O_{V_{2-1}\cap O_{V_2}}}^C$ that is

$$\mathcal{P}_{O_{V_2}}^{RF} = 1 - \mathcal{P}_{O_{V_2}}^C = 1 - \mathcal{P}_{O_{V_{2-1}\cap O_{V_2}}}^C, \quad (35)$$

$$\mathcal{P}_{O_{V_{2-1}\cap O_{V_2}}}^C =$$

$$\mathbb{P}\Big(\frac{\xi_1 P_{RF}G_tG_r\ell h_2||h^2 + r_2^2||^{-\frac{\alpha}{2}}}{\xi_2 P_{RF}G_tG_r\ell h_2||h^2 + r_2^2||^{-\frac{\alpha}{2}} + \mathcal{I}'_{RF}} > \zeta_1,$$
$$\frac{\xi_2 P_{RF}G_tG_r\ell h_2||h^2 + r_2^2||^{-\frac{\alpha}{2}}}{\mu\xi_1 P_{RF}G_tG_r\ell h_2||h^2 + r_2^2||^{-\frac{\alpha}{2}} + \mathcal{I}'_{RF}} > \zeta_2\Big),$$
$$= \mathbb{P}\Big(h_2 > \frac{\zeta_1 \mathcal{I}'_{\mathcal{RF}}}{(\xi_1 - \zeta_1\xi_2)P_{RF}G_tG_r\ell h_2||h^2 + r_2^2||^{-\frac{\alpha}{2}}}, \quad (36)$$
$$h_2 > \frac{\zeta_2 \mathcal{I}'_{\mathcal{RF}}}{(\xi_2 - \mu\zeta_2\xi_1)P_{RF}G_tG_r\ell h_2||h^2 + r_2^2||^{-\frac{\alpha}{2}}}\Big),$$
$$= \mathscr{L}_{I'_{RF}}\Big(\frac{J}{P_{RF}G_tG_r\ell h_2||h^2 + r_2^2||^{-\frac{\alpha}{2}}}\Big).$$

where $\zeta_2 = 2^{R_2} - 1$ and $J = \max(J_1, J_2)$. Here, $J_1 = \frac{\zeta_1}{(\xi_1 - \zeta_1\xi_2)}$ and $J_2 = \frac{\zeta_2}{(\xi_2 - \mu\zeta_2\xi_1)}$.

V-RF NOMA Extension to M-nodes

Here, we extend the V-RF NOMA results to M-destination nodes. We define the expression of the SIR at V_i to decode V_t message as follows

$$SIR_{V_i \to t} =$$

$$\frac{\xi_t P_{RF}G_tG_r\ell h_t||h^2 + r_i^2||^{-\frac{\alpha}{2}}}{P_{RF}G_tG_r\ell h_t||h^2 + r_i^2||^{-\frac{\alpha}{2}}\Big[\mu\sum_{k=1}^{t-1}\xi_k + \sum_{n=t+1}^{M}\xi_n\Big] + \mathcal{I}_{RF}^i}. \quad (37)$$

Same as above, when $k > t - 1$, then $\sum_{k=1}^{t-1}\xi_k = 0$ and when $n > M$, then $\sum_{n=t+1}^{M} = 0$. In this case, the outage probability, $\mathcal{P}_{O_{V_i}}$ can be expressed as $\mathcal{P}_{O_{V_i}}$

$$= \begin{cases} 1; & \text{if } \bigcup_{t=1}^{M}\frac{\xi_t}{\mu\sum_{k=1}^{t-1}\xi_k + \sum_{n=t+1}^{M}\xi_n} < \zeta_t, \\ 1 - \mathscr{L}_{I_{RF}^i}\Big(\frac{J_{(i)max}}{P_{RF}G_tG_r\ell h_t||h^2 + r_i^2||^{-\frac{\alpha}{2}}}\Big); & \text{if } otherwise, \end{cases} \quad (38)$$

where $J_{(i)max}$ is given by
$$J_{(i)max} =$$

$$\max\Bigg(\frac{\zeta_{i-(M-1)}}{\xi_{i-(M-1)} - \zeta_{i-(M-1)}\Big[\mu\sum_{k=1}^{i-(M-1)-1}\xi_k + \sum_{n=i-(M-1)+1}^{M}\xi_n\Big]},$$
$$\frac{\zeta_{i-(M-2)}}{\xi_{i-(M-2)} - \zeta_{i-(M-2)}\Big[\mu\sum_{k=1}^{i-(M-2)-1}\xi_k + \sum_{n=i-(M-2)+1}^{M}\xi_n\Big]}, ...,$$
$$\frac{\zeta_{i-(M-\ell)}}{\xi_{i-(M-\ell)} - \zeta_{i-(M-\ell)}\Big[\mu\sum_{k=1}^{i-(M-\ell)-1}\xi_k + \sum_{n=i-(M-\ell)+1}^{M}\xi_n\Big]}\Bigg). \quad (39)$$

where $\ell \in (1, 2,.., M)$.

C. Average Achievable Rate for V-VLC

In this subsection, we derive the expression for average achievable rate for V_1 and V_2. Using the fact that $\mathbb{E}[X] = \int_0^\infty \mathbb{P}[X > t]dt$ for real-valued random variables with non-negative support, the expression for $\mathcal{R}_{V_1}$ for OPD NOMA case may be modified as

$$\mathcal{R}_{V_1} = \int_0^\infty \mathbb{P}\Big[\frac{1}{2}\log_2(1 + \frac{e}{2\pi}SIR_{V_1}) > t\Big]dt,$$
$$= \int_{t=0}^{\frac{1}{2}\log_2(1+\frac{e}{2\pi}\frac{\xi_1}{\xi_2})}\mathbb{P}\Big[SIR_{V_1} > \frac{2\pi}{e}(2^{2t} - 1)\Big]dt, \quad (40)$$

$$= \int_t \mathbb{P}\Big[\mathcal{I}_{VLC} < \frac{k(\xi_1 - \xi_2\beta)P_{VLC}r_1^{2(m+1)}||h^2 + r_1^2||^{-(m+3)}}{\beta}\Big]dt, \quad (41)$$

$$= \int_t \mathcal{F}_{\mathcal{I}_{VLC}}\Big(\frac{k(\xi_1 - \xi_2\beta)P_{VLC}r_1^{2(m+1)}||h^2 + r_1^2||^{-(m+3)}}{\beta}\Big)dt. \quad (42)$$

where $\beta = \frac{2\pi}{e}(2^{2t} - 1)$ and $\mathcal{F}_{\mathcal{I}_{VLC}}(.)$ denotes the CDF of interference caused from V2V communication. The CDF expression has been derived in **Appendix B**.

The average achievable rate associated with vehicle V_2, denoted by $\mathcal{R}_{V_2}$ is represented as

$$\mathcal{R}_{V_2} = \mathbb{E}\Big[\frac{1}{2}\log_2(1 + \frac{e}{2\pi}SIR_{V_2})\Big], \quad (43)$$

Thus, the expression of $\mathcal{R}_{V_2}$ is given by

$$\mathcal{R}_{V_2} = \int_{t=0}^{\frac{1}{2}\log_2(1+\frac{e}{2\pi}\frac{\xi_2}{\mu\xi_1})}\mathbb{P}\Big[\frac{1}{2}\log_2(1 + \frac{e}{2\pi}SIR_{V_2}) > t\Big]dt, \quad (44)$$

$$= \int_t \mathcal{F}_{\mathcal{I}_{VLC}}\Big(\frac{k(\xi_2 - \xi_1\mu\beta)P_{VLC}r_2^{2(m+1)}||h^2 + r_2^2||^{-(m+3)}}{\beta}\Big)dt. \quad (45)$$

The expression of the average achievable rate at the user V_i when OPD NOMA is considered is given by

$$\mathcal{R}_{V_i} = \int_{t=0}^{v_{sup}} \mathcal{F}_{\mathcal{I}_{VLC}} \left(\frac{k(\xi_i - \beta[\mu \sum_{h=1}^{i-1} \xi_h + \sum_{n=i+1}^{M} \xi_n])}{\beta} \right.$$

$$\left. \times P_{VLC} r_i^{2(m+1)} ||h^2 + r_i^2||^{-(m+3)} \right) dt, \quad (46)$$

where $v_{sup} = \frac{1}{2} \log_2(1 + \frac{e}{2\pi} \frac{\xi_i}{\mu \sum_{h=1}^{i-1} \xi_h + \sum_{n=i+1}^{M} \xi_n})$.

For OMA case, the average achievable rate at the receiving node, V_i, denoted by $\mathcal{R}_{V_i}^{(OMA)}$, can be expressed as[3]

$$\mathcal{R}_{V_i}^{(OMA)} = \int_{t=0}^{\infty} \mathbb{P} \left[\frac{1}{4} \log_2(1 + \frac{e}{2\pi} SIR_{V_i}) > t \right] dt, \quad (47)$$

$$= \int_t \mathcal{F}_{\mathcal{I}_{VLC}} \left(\frac{k P_{VLC} r_i^{2(m+1)} ||h^2 + r_i^2||^{-(m+3)}}{\beta'} \right) dt. \quad (48)$$

where $\beta' = \frac{2\pi}{e}(2^{4t} - 1)$.

D. Average Achievable Rate for V-RF

In this case, the maximum achievable capacity for vehicle V_i is given as $\log_2(1 + SIR_{V_i})$. Following the similar steps as in OPD-NOMA, the average achievable rate associated with V_1 can be given as

$$\mathcal{R}_{V_1} = \int_{v=0}^{\log_2(1 + \frac{\xi_1}{\xi_2})} \mathbb{P}[SIR_{V_1} > 2^v - 1] dv, \quad (49)$$

$$= \int_v \mathscr{L}_{\mathcal{I}_{RF}} \left(\frac{2^v - 1}{(\xi_1 - (2^v - 1)\xi_2) P_{RF} G_t G_r \ell ||h^2 + r_1^2||^{-\frac{\alpha}{2}}} \right) dv. \quad (50)$$

Then, the average achievable rate related to V_2 can be expressed as

$$\mathcal{R}_{V_2} = \int_{v=0}^{\log_2(1 + \frac{\xi_2}{\mu \xi_1})} \mathbb{P}[SIR_{V_2} > 2^v - 1] dv, \quad (51)$$

$$= \int_v \mathscr{L}_{\mathcal{I}_{RF}} \left(\frac{2^v - 1}{(\xi_2 - (2^v - 1)\mu \xi_1) P_{RF} G_t G_r \ell ||h^2 + r_2^2||^{-\frac{\alpha}{2}}} \right) dv. \quad (52)$$

The average achievable rate associated with vehicle V_i, denoted by $\mathcal{R}_{V_i}$ can be expressed as

$$\mathcal{R}_{V_i} = \int_0^{v_{sup}} \mathscr{L}_{\mathcal{I}_{RF}} \left(\frac{2^v - 1}{(\xi_i - \beta \left[\mu \sum_{h=1}^{i-1} \xi_h + \sum_{n=i+1}^{M} \xi_n \right])} \right.$$

$$\left. \times \frac{1}{P_{RF} G_t G_r \ell ||h^2 + r_2^2||^{-\frac{\alpha}{2}}} \right) dv. \quad (53)$$

where $\beta = 2^v - 1$ and $v_{sup} = \log_2(1 + \frac{\xi_i}{\mu \sum_{h=1}^{i-1} \xi_h + \sum_{n=i+1}^{M} \xi_n})$.

Again for OMA case, the average achievable rate at the receiving node, V_i, denoted by $\mathcal{R}_{V_i}^{(OMA)}$, can be expressed as

$$\mathcal{R}_{V_i}^{(OMA)} = \int_{v=0}^{\infty} \mathscr{L}_{\mathcal{I}_{RF}} \left(\frac{2^{2v} - 1}{P_{RF} G_t G_r \ell ||h^2 + r_i^2||^{-\frac{\alpha}{2}}} \right) dv. \quad (54)$$

[3]Notice that the achievable rate is multiplied by $\frac{1}{2}$ since we assume bandwidth splitting in OMA.

IV. Numerical Results and Discussion

In this section, we present results that corroborate our theoretical findings. The system model parameters used for the analysis are summarized in Table I. We present the down link performance of OPD-NOMA with perfect SIC as well as error propagation due to imperfect SIC in presence of several system model parameters. The distance between transmitter and receiver is set to $||S - V_1|| = 40$ m and $||S - V_2|| = 47$ m. In order to validate the accuracy of our theoretical findings, Monte Carlo simulations are performed by averaging over 10,000 realizations of PPPs and fading channel parameters[4]. We consider a worst case scenario where interference from V2V arise from infinite road segment ($\mathcal{B} = \mathbb{R}^1$).

TABLE I: System Model Parameters

Parameter	Symbol	Value
Lambertian Order	m	1 [43]
PD active detection area	A_d	$1\ cm^2$ [43]
LED semi-angle	$\Phi_{\frac{1}{2}}$	$70°$
Transmission power for VLC	P_{VLC}	33 dBm [39]
VLC System Bandwidth	B_s	20 MHz
Responsivity of the PD	$\mathcal{R}$	0.54 A/W [43]
Absolute temperature	T_k	$298°$ K
Transmission power for VLC	P_{VLC}	23 dBm [39]
RF System Bandwidth	B_s	10 MHz
Transmitter antenna gain	G_t	3dBi
Receiver antenna gain	G_r	3dBi
Optical filter gain	$T_s(\Psi_k)$	1
Noise power spectral density	N_o	$10^{-21} A^2/Hz$
Refractive index	n	1.5
Path loss exponent	α	2
Power allocation coefficient	ζ	0.5-1
Inter-lane spacing	L	10 m [39]
Height of RSU	h	10 m

Fig. 4 shows the relationship between outage probability of OPD NOMA and vehicular density, λ. We set power allocation coefficient, ξ_1 and access probability ϱ to be 0.85 and 0.02 respectively. Keeping in view different data requirement by each user, the target data rate of V_2 is assumed to be greater than V_1. It can be observed from Fig. 4 that as expected, the outage probability increases as vehicular density increases. We also compare the OMA and NOMA systems for the case of two users. We can observe that the outage performance of each vehicle of OPD NOMA system is superior to OMA system for vehicle V_1 as well as V_2. This is due to fact that the diversity order of the NOMA system is typically higher than OMA system [44]. In order to evaluate the potential trade off between OPD-NOMA based V-VLC systems and V-RF systems, we compare our result with conventional V-RF

[4]The Monte carlo simulation procedure are described as follows. It may be noted that the vehicles are deployed over a length of 10,000 m, and the interference is summed at the origin as per (12) and preserved. The scenario is repeated for at least 10,000 times in order to obtain the statistics of the interference. Given our simulation settings, we further calculate the SIR as per (11) and (14) and count the number of times for which SIR not larger than the threshold β, accordingly the simulated outage probability is computed as:

$$\hat{\mathcal{P}_O} = \frac{\sum_{m=1}^{N} 1_{SIR \leq \beta}}{N} \quad (55)$$

where N denotes the total number of simulation runs respectively. The simulation has been performed using the `MATLAB` software.
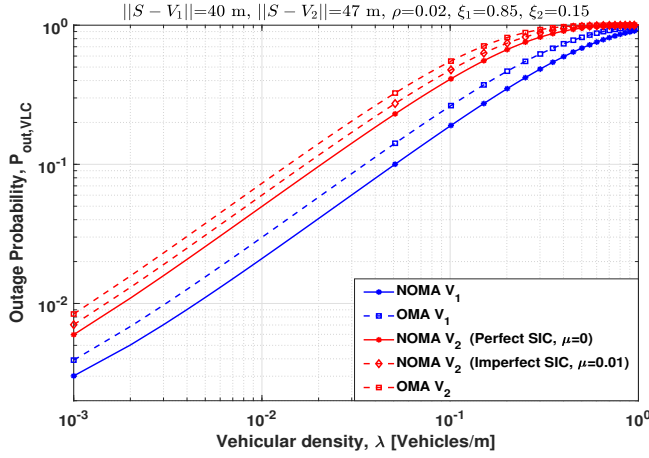
Fig. 4: Outage Probability, $\mathcal{P}_{out,VLC}$ as a function of vehicular density, λ considering OPD NOMA (solid line) and OMA (dashed line) for V-VLC communication.
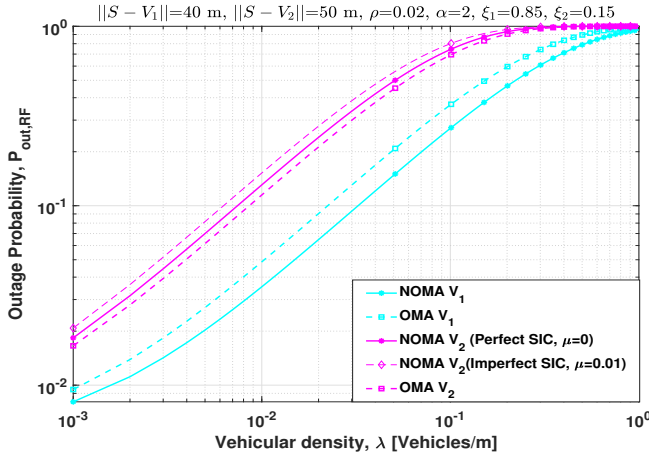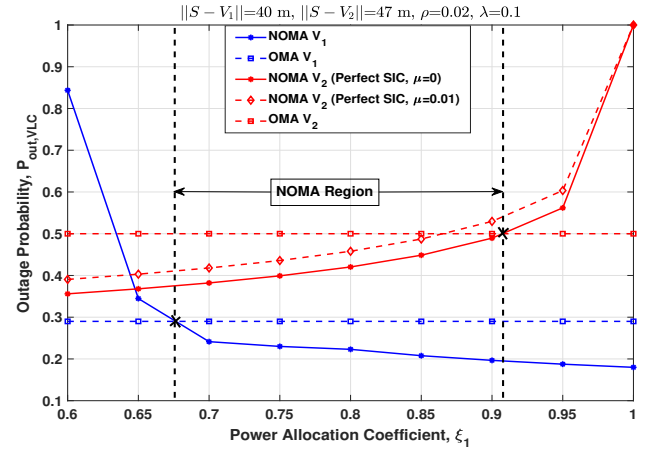

Fig. 6: Outage performance of V-VLC as a function of power allocation coefficient, ξ_1 for OMA (dashed) and NOMA(solid).

Fig. 5: Outage Probability, $\mathcal{P}_{out,RF}$ as a function of vehicular density, λ considering NOMA (solid line) and OMA (dashed line) for V-RF communication.

OMA and NOMA system. It is noteworthy that the outage performance of NOMA is sensitive to the values of power allocation coefficient, source-destination distance and target data rate threshold.

Fig. 5 depicts outage probability as a function of vehicular density for V-RF communication. Again similar insights can be obtained. Surprisingly, OMA system is superior than that of NOMA system for UE-2. As mentioned before, the power allocation coefficient, ξ_1 indeed affects the outage performance. Interestingly, a suitable choice of power allocation coefficient decides the NOMA outage probability. For ease of validation and visualization, we also plot outage probability, $\mathcal{P}_{out,VLC}$ as a function of power allocation coefficient, ξ_1 as can be seen in Fig. 6 and 7.

From Fig. 6, we notice that in OPD NOMA, when power allocation coefficient, ξ_1 increases, $\mathcal{P}_{O_{V_1}}$ decreases, while $\mathcal{P}_{O_{V_2}}$ increases. Next, if we compare NOMA and OMA outage performance, we observe that, for V_1, OMA performs better as compared to NOMA when $\xi_1 \in [0.6, 0.67]$. This is mainly

because lower values of ξ_1 means low power is being allocated to V_1, while high power is allocated to V_2 which increases the interference at V_1. Conversely, we can observe that when $\xi_1 \in [0.67, 1]$, OPD NOMA performs superior as compared to OMA. This is due to the fact that V_1 is allocated more power, while less power is allocated to V_2. For V_2, we see that OMA outperforms NOMA only when $\xi_1 \in [0.91, 1]$. This is true because, for large values of ξ_1, V_2 is allocated a small amount of power, thus decreasing the SIR at V_2 and results in increased outage probability. In nutshell, both users exhibit superior NOMA performance over OMA system when $\xi_1 \in [0.67, 0.91]$. In fact, OPD NOMA offers quite wider choice of power allocation coefficient as compared to V-RF NOMA as evident from Fig. 6.

We can observe from Fig. 7 that for V_1, when $\xi_1 \in [0.66, 1]$, V-RF NOMA outperforms V-RF OMA system. On other hand, for V_2, when $\xi_1 < 0.8$, V-RF NOMA outperforms V-RF OMA system. It can be noted that the benefit of NOMA over OMA system can be exploited when $\xi_1 \in [0.66, 0.8]$. However, with error propagation due to imperfect SIC ($\mu = 0.01$), the range of ξ_1 shrinks to $[0.68, 0.76]$.

Next, we compare NOMA performance for V-VLC and V-RF link depending on location of far-off users. We can observe from Fig. 8 that when location of far-off NOMA user from source, $||S - V_2||$ increases, outage probability also increases. Also, the outage performance of standalone V-VLC link is comparatively better than standalone V-RF for low communication range. For instance, when interfering vehicular density, $\lambda = 0.01$, the outage performance of V-VLC link is better compared to V-RF Link when distance of far-off NOMA user from source, $||S - V_2||$ is upto 80 m. However, V-RF is reliable option for long distance communication. In nutshell, there exists tradeoff between NOMA based V-VLC and V-RF link depending upon the location of NOMA user from source.

We now show the impact of residual interference after SIC process, μ on outage performance of standalone V-VLC and V-RF link. We see from Fig. 9 that as residual interference fraction, μ increases, $\mathcal{P}_{out}$(outage probability) also increases.
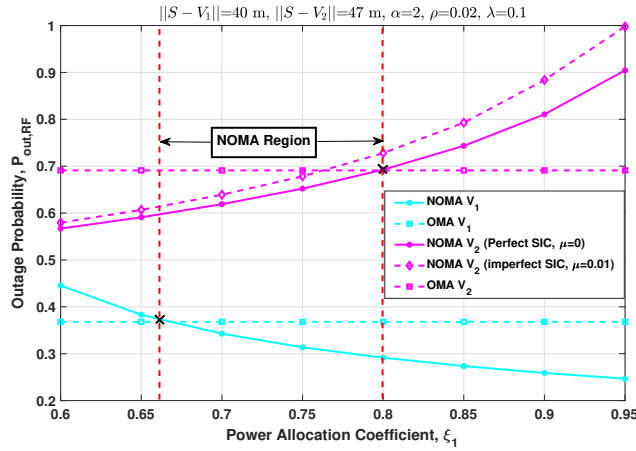
Fig. 7: Outage performance of V-RF as a function of power allocation coefficient, ξ_1 for OMA (dashed) and NOMA (solid).
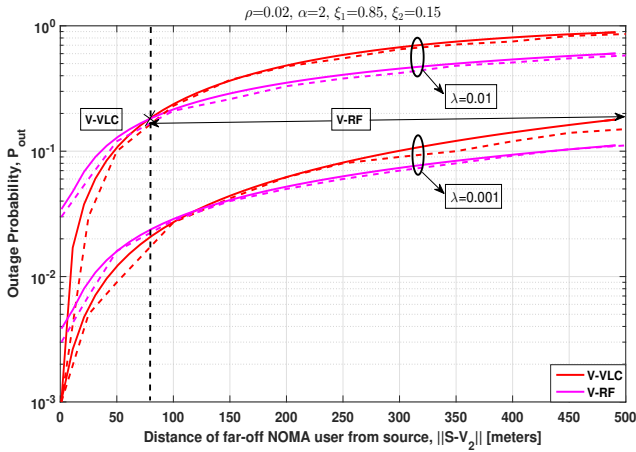

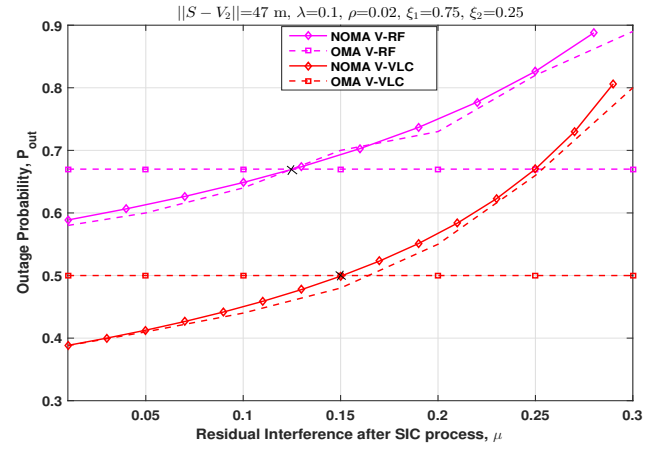
Fig. 8: Comparison of analytical (solid line) and simulation (dashed line) results for outage probability, $\mathcal{P}_{out}$ versus distance of far-off NOMA user for OPD NOMA based V-VLC link (red) and NOMA based V-RF link (magenta)

Fig. 9: Comparison of analytical (solid line) and simulation (dashed line) results for outage probability, $\mathcal{P}_{out}$ as a function of interference fraction left after SIC process for OPD NOMA based V-VLC link (red) and NOMA based V-RF link (magenta)
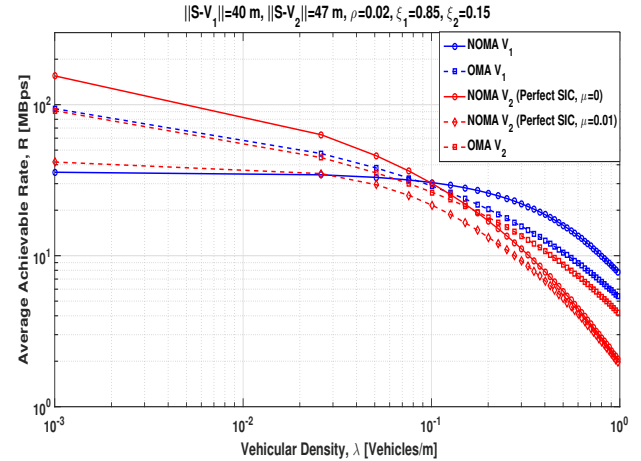

Fig. 10: Average achievable rate, $\mathcal{R}$ variation with vehicular density, λ considering OMA (dashed line) and NOMA (solid line) for V-VLC communication.

We can observe that NOMA exhibits better performance than OMA when $\mu<0.15$ and $\mu<0.13$ for V-VLC and V-RF respectively. In other words, there is no advantage of using OPD NOMA when more than 15% of interference related to V_1 is not completely removed. Similarly, there is no benefit of using NOMA based V-RF link when more than 13% of interference related to V_1 is not removed. It should be noted here that this is a critical system design parameter for both VLC as well as RF based NOMA vehicular systems.

Fig. 10 illustrates the relationship between average achievable rate and vehicular density, λ. We observe that the vehicle V_2 has a larger average achievable rate than V_1. This is due to the fact that V_2 does not experience extra interference. In contrast, this trend holds true only for low values of vehicular density. For high vehicular density, the performance of V_2 decreases drastically. We can also observe that V_1 are more robust to the interference for higher values of λ. For such highly dense environment ($\lambda > 0.1$), V_1 has better achievable

rate than V_2.

Fig. 11 shows average achievable rate as a function of vehicular density, λ for V-RF communication. Again, the average achievable rate for V_2 is larger than V_1 for low vehicular density. In comparison with OPD NOMA, irrespective of traffic intensity, V-RF NOMA has always lower average achievable rate for both the users especially for lower values of vehicular density ($\lambda < 0.1$). It should be noted again that the average achievable rate also depends on power allocation coefficient, source- destination distance and target rate thresholds.

Next, we plot the behaviour of average achievable rate variation with power allocation coefficient, ξ_1 in Fig. 12. We observe from Fig. 14 that in OPD NOMA, when power allocation coefficient, ξ_1 increases, $\mathcal{R}_{V_2}$ decreases, while $\mathcal{R}_{V_1}$ increases. In particular when $\xi_1 < 0.8$, average achievable rate of V_2 with OPD NOMA is greater than OMA. When $\xi_1 > 0.54$, OPD NOMA exhibits better performance as
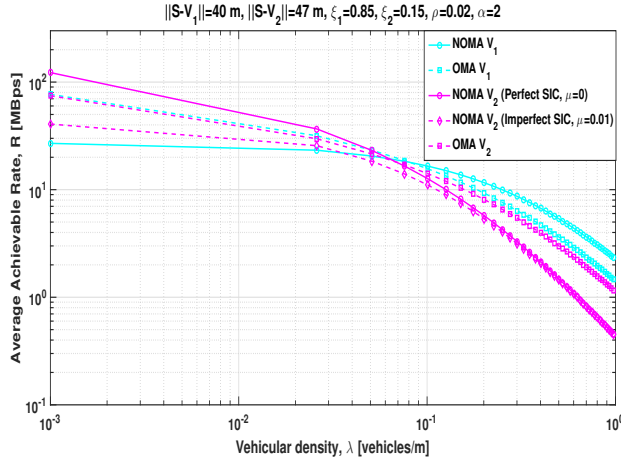
Fig. 11: Average achievable rate, $\mathcal{R}$ variation with vehicular density, λ considering OMA (dashed line) and NOMA (solid line) for V-RF communication.
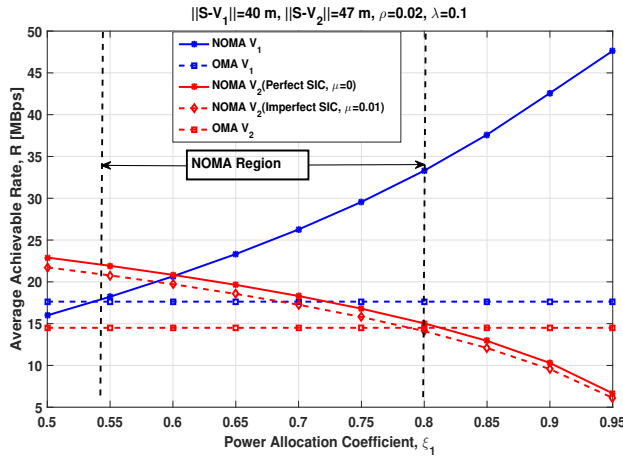

Fig. 12: Average achievable rate, $\mathcal{R}$ of V-VLC as a function of power allocation coefficient, ξ_1 for OMA (dashed) and NOMA (solid line).

compared to OMA in terms of average achievable rate for V_1. This implies that as ξ_1 increases, V_1 is allocated more power, while less power is allocated to V_2, therefore the average achievable rate of V_1 increases, on other hand, the average achievable rate of V_2 decreases. At same time, we can also observe that when $\xi_1 \in [0.54, 0.8]$, OPD NOMA could able to achieve better average rate for both V_1 and V_2 as compared to OMA system.

For comparison purpose, we also plot the average achievable rate as a function of power allocation coefficient for V-RF communication. We can observe from Fig. 13 that when $\xi_1 \in [0.8, 0.85]$, NOMA achieves better average rate for both V_1 and V_2 compared to OMA system.

V. CONCLUDING REMARKS

In this paper, we explore the potential benefit and research challenges involved with practical implementation of downlink OPD NOMA based V2X network for broadcasting road safety related information. We compare the performance of proposed
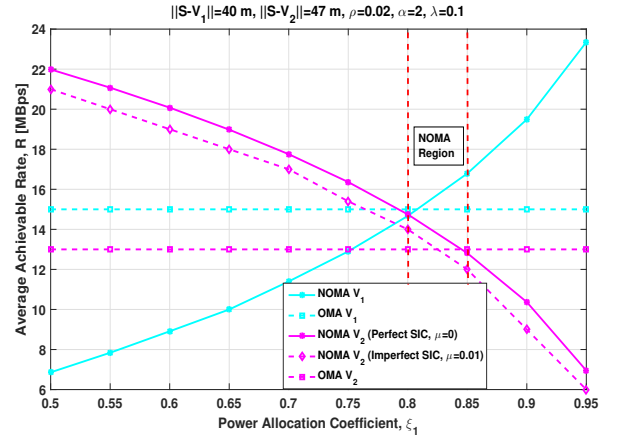

Fig. 13: Average achievable rate, $\mathcal{R}$ of V-RF as a function of power allocation coefficient, ξ_1 for NOMA(solid) and OMA (dashed).

downlink OPD NOMA based V2X network with OMA system using stochastic geometry tools. We show that the proposed OPD NOMA based V2X network offers improved performance in terms of outage performance, and average achievable rate as compared to conventional RF NOMA based V2X network. However, there also exists tradeoff between NOMA based V-VLC and V-RF link depending upon the location of NOMA user from source.

It may be noted that several open research challenges such as power imbalance among vehicles, impact of channel symmetry, power allocation techniques under feedback delay, synchronization in a high-mobility scenario, non linear distortion in OPD-NOMA, co-existence of V-VLC and V-RF, etc are yet to be explored. However, we believe that the presented contribution may serve as a valuable resource for future invention, optimal planning and development of next generation VLC based intelligent transportation system. Undoubtedly, uplink OPD NOMA can be a potential future direction of research for beyond 5G enabled V2X network.

APPENDIX A

The Laplace transform, $\mathscr{L}_{I_{RF}}(s)$ can be computed as:

$$\mathscr{L}_{I_{RF}}(s) = \mathbb{E}[\exp(-sI_{RF}]$$

$$= \mathbb{E}\left[\prod_r \exp(-sP_{RF}G_tG_r\ell h||r'||^{-\alpha})\right]$$

$$\overset{(a)}{=} \mathbb{E}_r\left[\prod_r \mathbb{E}_h\{\exp(-sP_{RF}G_tG_r\ell h||r||^{-\alpha})\}\right]$$

$$= \mathbb{E}_r\left[\prod_r \frac{1}{1+sP_{RF}G_tG_r\ell||r'||^{-\alpha}}\right]$$

$$\overset{(b)}{=} \exp\left(-\varrho\lambda\int_{r_1}^{\infty}\frac{1}{1+||r'||^{\alpha}/sP_{RF}G_tG_r\ell}dr\right)$$

$$\overset{(c)}{=} \exp\left(-\varrho\lambda(sP_{RF}G_tG_r\ell)^{\frac{1}{\alpha}}\int_{r_1}^{\infty}\frac{1}{1+v^{\alpha}}dv\right)$$

$$\overset{(d)}{=} \exp\left(-\varrho\lambda(sP_{RF}G_tG_r\ell)^{\frac{1}{\alpha}}\frac{\pi}{\alpha}\csc(\frac{\pi}{\alpha})\right)$$

$$\tag{56}$$

here, (a) holds due to independence of channel fading co-efficients h_x and assumes $L << r'$, (b) uses the PGFL for Homogeneous PPP , (c) involves variable transformation $||r||/(sP_{RF}G_tG_r\ell)^{\frac{1}{\alpha}} \to v$, and (d) when $r_1 \to 0$. Substituting $s = \frac{\zeta_1}{(\xi_1 - \zeta_1\xi_2)P_{RF}G_tG_r\ell||h^2+r_1^2||^{-\frac{\alpha}{2}}}$ yields the desired result

$$\mathscr{L}_{I_{RF}}\left(\frac{\zeta_1}{(\xi_1 - \zeta_1\xi_2)P_{RF}G_tG_r\ell||h^2 + r_1^2||^{-\frac{\alpha}{2}}}\right) = \exp\left(-\varrho\lambda\left(\frac{\zeta_1}{(\xi_1 - \zeta_1\xi_2)}\right)^{\frac{1}{\alpha}}||h^2 + r_1^2||^{\frac{1}{2}}\frac{\pi}{\alpha}\csc(\frac{\pi}{\alpha})\right). \tag{57}$$

APPENDIX B

In order to obtain the the interference distribution, we first calculate its characteristics function (CF) denoted as $\varphi_{\mathcal{I}}$. By definition, the CF of a random variable X is given as $\mathbb{E}\left[e^{j\omega X}\right]$.

$$\varphi_I(\omega) = \mathbb{E}\left[e^{j\omega I}\right],$$
$$= \underset{r\in\Psi_{PPP}}{\mathbb{E}}\left[\exp(j\omega\sum_{r\in\Psi_{PPP}} kP_{VLC}\frac{r'^{2(m+1)}}{(L^2 + r'^2)^{m+\gamma+1}}\right],$$
$$= \underset{r\in\Psi_{PPP}}{\mathbb{E}}\left[\prod_{r\in\Psi_{PPP}}\exp(j\omega kP_{VLC}\frac{r'^{2(m+1)}}{(L^2 + r'^2)^{m+\gamma+1}})\right], \tag{58}$$

The expectation in Eq. (58) can be solved using definition of PGFL for homogeneous PPP over region of interest, $\mathcal{R}$ [24, Th 4.9]. Eq.(58) can be rewritten as

$$\varphi_{\mathcal{I}}(\omega) = \exp\left(-\int_{r_1}^{\infty}\left[1 - \exp\left(\frac{j\omega kP_{VLC}r^{2(m+1)}}{(L^2 + r^2)^{m+\gamma+1}}\right)\right]\varrho\lambda dr\right), \tag{59}$$

Now we make use of Gil-Peleaz's inversion theorem to numerically evaluate the CDF [45].

$$F_{\mathcal{I}}(x) = \frac{1}{2} - \frac{1}{\pi}\int_0^{\infty}\frac{1}{\omega}\Im\left[\varphi_{\mathcal{I}}(\omega)e^{-j\omega x}\right]d\omega, \tag{60}$$

To simplify the calculation, we assume that the inter-lane distance, L can be ignored as compared to the longitudinal stretch of the road, r. With no loss of generality, we can further simplify the above CF by assuming the value of path loss exponent ($\gamma' = 2$) and $r_1 \to 0$, thus (59) simplifies to a more closed form as:

$$\varphi_{\mathcal{I}}(\omega) = \exp\left(-\left[\varrho\lambda\Gamma(1 - \frac{1}{\gamma'})(-jkP_{VLC}\omega)^{\frac{1}{\gamma'}}\right]\right),$$
$$= \exp\left(-\sqrt{-j\pi kP_{VLC}\omega(\varrho\lambda)^2}\right), \tag{61}$$

The above equation can be compared with more tractable inverse gamma distribution (also called Levy-distribution) having a CF and a CDF of the form:

$$\varphi(\omega) = e^{\left(j\mu\omega - \sqrt{-2ja\omega}\right)},$$
$$F_X(x) = \xi_c\left(\sqrt{\frac{a}{2(x - \mu)}}\right), \tag{62}$$

where ξ_c, μ and a denote the complementary error function, the location parameter and the scale parameter respectively. On comparing Eq.(61) with Eq.(62), we can conclude that CF follows a Levy distribution with CDF of the form as given below:

$$F_{\mathcal{I}_{VLC}}(x) = \xi_c\left(\sqrt{\frac{\pi(\varrho\lambda)^2 kP_{VLC}}{4x}}\right). \tag{63}$$

ACKNOWLEDGMENT

REFERENCES

[1] M. Z. Chowdhury, M. T. Hossan, A. Islam, and Y. M. Jang, "A Comparative Survey of Optical Wireless Technologies: Architectures and Applications," *IEEE Access*, vol. 6, pp. 9819–9840, 2018.

[2] L. Z. Rahim, Md. Noor, H. Lee, M. O. Khyam, J. He, D. Pesch, K. Moessner, W. Saad, H. V. Poor *et al.*, "6g for vehicle-to-everything (v2x) communications: Enabling technologies, challenges, and opportunities," *arXiv preprint arXiv:2012.07753*, 2020.

[3] M. Liaqat, K. A. Noordin, T. A. Latef, and K. Dimyati, "Power-Domain Non Orthogonal Multiple Access (PD-NOMA) in Cooperative Networks: an Overview," *Wireless Networks*, pp. 1–23, 2018.

[4] B. Di, L. Song, Y. Li, and Z. Han, "V2X meets NOMA: Non-Orthogonal Multiple Access for 5G-Enabled Vehicular Networks," *IEEE Wireless Commun.*, vol. 24, no. 6, pp. 14–21, Dec 2017.

[5] H. Marshoud, V. M. Kapinas, G. K. Karagiannidis, and S. Muhaidat, "Non-Orthogonal Multiple Access for Visible Light Communications," *IEEE Photonics Technology Letters*, vol. 28, no. 1, pp. 51–54, Jan 2016.

[6] L. Yin, W. O. Popoola, X. Wu, and H. Haas, "Performance Evaluation of Non-Orthogonal Multiple Access in Visible Light Communication," *IEEE Trans. Commun.*, vol. 64, no. 12, pp. 5162–5175, 2016.

[7] X. Guan, Q. Yang, Y. Hong, and C. C.-K. Chan, "Non-Orthogonal Multiple Access with Phase Pre-Distortion in Visible Light Communication," *Optics express*, vol. 24, no. 22, pp. 25 816–25 823, 2016.

[8] Y. Fu, Y. Hong, L.-K. Chen, and C. W. Sung, "Enhanced Power Allocation for Sum Rate Maximization in OFDM-NOMA VLC systems," *IEEE Photonics Technology Letters*, vol. 30, no. 13, pp. 1218–1221, 2018.

[9] C. Chen, W.-D. Zhong, H. Yang, and P. Du, "On the Performance of MIMO-NOMA-Based Visible Light Communication Systems," *IEEE Photonics Technology Letters*, vol. 30, no. 4, pp. 307–310, 2017.

[10] N. DOCOMO, "Initial Views and Evaluation Results on Non-Orthogonal Multiple Access for NR," in *R1-165175, 3GPP TSG RAN WG1 Meeting*, vol. 85, 2016.

[11] W. Roh, "5G mobile communications for 2020 and beyond-vision and key enabling technologies," *Key note: at IEEE WCNC*, 2014.

[12] Y. Saito, Y. Kishiyama, A. Benjebbour, T. Nakamura, A. Li, and K. Higuchi, "Non-Orthogonal Multiple Access (NOMA) for Cellular Future Radio Access," in *Proc. IEEE 77th vehicular technology conference (VTC Spring)*. IEEE, 2013, pp. 1–5.

[13] Z. Ghassemlooy, W. Popoola, and S. Rajbhandari, *Optical wireless communications: system and channel modelling with Matlab®*. CRC press, 2019.

[14] Y. S. Eroğlu, İ. Güvenç, A. Şahin, Y. Yapıcı, N. Pala, and M. Yüksel, "Multi-element VLC networks: LED assignment, power control, and optimum combining," *IEEE J. Selected Areas Commun.*, vol. 36, no. 1, pp. 121–135, 2017.

[15] S. I. Mushfique, P. Palathingal, Y. S. Eroglu, M. Yuksel, I. Guvenc, and N. Pala, "A software-defined multi-element VLC architecture," *IEEE Commun. Mag.*, vol. 56, no. 2, pp. 196–203, 2018.

[16] H. Burchardt, N. Serafimovski, D. Tsonev, S. Videv, and H. Haas, "VLC: Beyond point-to-point communication," *IEEE Commun. Mag.*, vol. 52, no. 7, pp. 98–105, 2014.

[17] D. Tsonev, H. Chun, S. Rajbhandari, J. J. McKendry, S. Videv, E. Gu, M. Haji, S. Watson, A. E. Kelly, G. Faulkner *et al.*, "A 3-gb/s single-LED OFDM-based wireless VLC link using a gallium nitride," *IEEE Photonics Technology Letters*, vol. 26, no. 7, pp. 637–640, 2014.

[18] B. Lin, W. Ye, X. Tang, and Z. Ghassemlooy, "Experimental demonstration of bidirectional noma-ofdma visible light communications," *Optics express*, vol. 25, no. 4, pp. 4348–4355, 2017.

[19] B. Lin, Z. Ghassemlooy, X. Tang, Y. Li, and M. Zhang, "Experimental demonstration of optical MIMO NOMA-VLC with single carrier transmission," *Optics Communications*, vol. 402, pp. 52–55, 2017.

[20] D. Tweed, S. Parsaeefard, M. Derakhshani, and T. Le-Ngoc, "Dynamic resource allocation for mc-noma vwns with imperfect sic," in *Proc. IEEE 28th Annual International Symposium on Personal, Indoor, and Mobile Radio Communications (PIMRC)*, 2017, pp. 1–5.

[21] X. Li, M. Liu, C. Deng, P. T. Mathiopoulos, Z. Ding, and Y. Liu, "Full-duplex cooperative NOMA relaying systems with i/q imbalance and imperfect sic," *IEEE Wireless Communications Letters*, vol. 9, no. 1, pp. 17–20, 2019.

[22] L. Chen, B. Cao, R. Lu, and Q. Zhang, "Joint resource allocation in NOMA systems with imperfect sic," in *Proc. IEEE Global Communications Conference (GLOBECOM)*, 2019, pp. 1–6.

[23] F. Baccelli and B. Błaszczyszyn, *Stochastic geometry and wireless networks*. Now Publishers Inc, 2009, vol. 1.

[24] M. Haenggi, *Stochastic Geometry for Wireless Networks*. Cambridge University Press, 2012.

[25] M. J. Farooq, H. ElSawy, and M.-S. Alouini, "Modeling inter-vehicle communication in multi-lane highways: A stochastic geometry approach," in *Proc. IEEE 82nd Vehicular Technology Conference (VTC2015-Fall)*, 2015, pp. 1–5.

[26] J. G. Andrews, F. Baccelli, and R. K. Ganti, "A tractable approach to coverage and rate in cellular networks," *IEEE Trans. commun.*, vol. 59, no. 11, pp. 3122–3134, 2011.

[27] S. N. Chiu, D. Stoyan, W. S. Kendall, and J. Mecke, *Stochastic geometry and its applications*. John Wiley & Sons, 2013.

[28] Z. Tong, H. Lu, M. Haenggi, and C. Poellabauer, "A stochastic geometry approach to the modeling of DSRC for vehicular safety communication," *IEEE Trans. Intell. Transport. Syst.*, vol. 17, no. 5, pp. 1448–1458, 2016.

[29] M. Obeed, A. M. Salhab, M.-S. Alouini, and S. A. Zummo, "On optimizing VLC networks for downlink multi-user transmission: A survey," *IEEE Comm. Surveys & Tutorials*, vol. 21, no. 3, pp. 2947–2976, 2019.

[30] R. C. Kizilirmak, C. R. Rowell, and M. Uysal, "Non-orthogonal multiple access (NOMA) for indoor visible light communications," in *Proc. IEEE 4th International Workshop on optical Wireless Communications (IWOW)*, 2015, pp. 98–101.

[31] W. U. Khan, F. Jameel, N. Kumar, R. Jäntti, and M. Guizani, "Backscatter-enabled efficient v2x communication with non-orthogonal multiple access," *IEEE Trans. Veh. Tech.*, vol. 70, no. 2, pp. 1724–1735, 2021.

[32] B. Di, L. Song, Y. Li, and Z. Han, "V2X meets NOMA: Non-orthogonal multiple access for 5g-enabled vehicular networks," *IEEE Wireless Communications*, vol. 24, no. 6, pp. 14–21, 2017.

[33] E. Steinmetz, M. Wildemeersch, T. Q. Quek, and H. Wymeersch, "Packet reception probabilities in vehicular communications close to intersections," *IEEE Transactions on Intelligent Transportation Systems*, 2020.

[34] B. E. Y. Belmekki, A. Hamza, and B. Escrig, "Performance analysis of cooperative communications at road intersections using stochastic geometry tools," *arXiv preprint arXiv:1807.08532*, 2018.

[35] C.-S. Choi and F. Baccelli, "An analytical framework for coverage in cellular networks leveraging vehicles," *IEEE Transactions on Communications*, vol. 66, no. 10, pp. 4950–4964, 2018.

[36] T. Komine and M. Nakagawa, "Fundamental Analysis for Visible-Light Communication System using LED lights," *IEEE Trans. on Consumer Electronics*, vol. 50, no. 1, pp. 100–107, 2004.

[37] Z. Ding, H. Dai, and H. V. Poor, "Relay selection for cooperative NOMA," *IEEE Wireless Commun. Lett.*, vol. 5, no. 4, pp. 416–419, 2016.

[38] Z. Ding, L. Dai, and H. V. Poor, "MIMO-NOMA design for small packet transmission in the internet of things," *IEEE access*, vol. 4, pp. 1393–1405, 2016.

[39] G. Singh, A. Srivastava, and V. A. Bohara, "Stochastic geometry-based interference characterization for RF and VLC-based vehicular communication system," *IEEE Syst. J.*, pp. 1–11, 2020.

[40] C. A. O'cinneide, "Euler Summation for Fourier series and Laplace Transform Inversion," *Stochastic Models*, vol. 13, no. 2, pp. 315–337, 1997.

[41] J. Abate and W. Whitt, "Numerical Inversion of Laplace Transforms of Probability Distributions," *ORSA Journal on computing*, vol. 7, no. 1, pp. 36–43, 1995.

[42] A. Goldsmith, *Wireless Communications*. Cambridge university press, 2005.

[43] P. Luo, Z. Ghassemlooy, H. Le Minh, E. Bentley, A. Burton, and X. Tang, "Fundamental analysis of a car to car visible light communication system," in *Proc. IEEE 9th International Symposium on Communication Systems, Networks & Digital Sign (CSNDSP)*, 2014, pp. 1011–1016.

[44] K. Janghel and S. Prakriya, "Performance of adaptive OMA/cooperative-NOMA scheme with user selection," *IEEE Communications Letters*, vol. 22, no. 10, pp. 2092–2095, 2018.

[45] J. Gil-Pelaez, "Note on the inversion theorem," *Biometrika*, vol. 38, no. 3-4, pp. 481–482, Dec. 1951.